

UC Irvine

UC Irvine Previously Published Works

Title

Under What Conditions Can Equilibrium Gas-Particle Partitioning Be Expected to Hold in the Atmosphere?

Permalink

<https://escholarship.org/uc/item/1q16b592>

Journal

ENVIRONMENTAL SCIENCE & TECHNOLOGY, 49(19)

ISSN

0013-936X

Authors

Mai, H
Shiraiwa, M
Flagan, RC
et al.

Publication Date

2015-10-06

DOI

10.1021/acs.est.5b02587

Peer reviewed

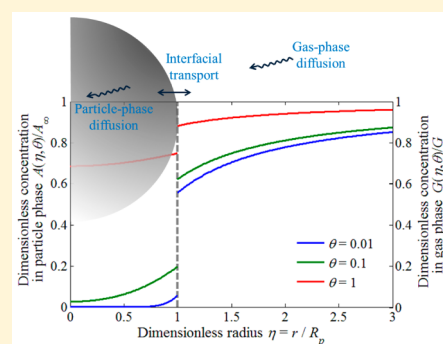
Under What Conditions Can Equilibrium Gas–Particle Partitioning Be Expected to Hold in the Atmosphere?

Huajun Mai,[†] Manabu Shiraiwa,[§] Richard C. Flagan,^{†,‡} and John H. Seinfeld^{*,†,‡}

[†]Division of Engineering and Applied Science and [‡]Division of Chemistry and Chemical Engineering, California Institute of Technology, Pasadena, California 91125, United States

[§]Multiphase Chemistry Department, Max Planck Institute for Chemistry, 55128 Mainz, Germany

ABSTRACT: The prevailing treatment of secondary organic aerosol formation in atmospheric models is based on the assumption of instantaneous gas–particle equilibrium for the condensing species, yet compelling experimental evidence indicates that organic aerosols can exhibit the properties of highly viscous, semisolid particles, for which gas–particle equilibrium may be achieved slowly. The approach to gas–particle equilibrium partitioning is controlled by gas-phase diffusion, interfacial transport, and particle-phase diffusion. Here we evaluate the controlling processes and the time scale to achieve gas–particle equilibrium as a function of the volatility of the condensing species, its surface accommodation coefficient, and its particle-phase diffusivity. For particles in the size range of typical atmospheric organic aerosols (~50–500 nm), the time scale to establish gas–particle equilibrium is generally governed either by interfacial accommodation or particle-phase diffusion. The rate of approach to equilibrium varies, depending on whether the bulk vapor concentration is constant, typical of an open system, or decreasing as a result of condensation into the particles, typical of a closed system.



1. INTRODUCTION

Mounting evidence indicates that organic aerosols can exhibit the properties of viscous, semisolid particles.^{1–12} In describing the process of formation of secondary organic aerosol (SOA), it has traditionally been assumed that condensing, low-volatility oxidation products partition according to instantaneous gas–particle equilibrium.¹³ The assumption of instantaneous gas–particle equilibrium implies that the time scale to achieve that equilibrium is short when compared to the time scales over which other processes, such as gas- and particle-phase dynamics, are occurring. Moreover, most current atmospheric chemical transport models incorporate the assumption of instantaneous gas–particle equilibrium in describing SOA formation. A consequence of a highly viscous aerosol phase is that gas–particle equilibrium for condensing species may not be established instantaneously, owing to the time associated with the transport processes in the gas phase, across the gas–particle interface, and within the particle itself. In this case, a dynamic, rather than equilibrium, formulation of the SOA formation process is required. Because the computational implications of dynamic versus equilibrium model formulations are significant, it is important to assess the conditions under which such a dynamic formulation is needed.

Several recent studies have addressed the time scales associated with the establishment of atmospheric gas–aerosol equilibrium. Shiraiwa and Seinfeld¹⁴ estimated the equilibration time scale of SOA gas–particle partitioning using a state-of-the-art numerical gas- and particle-phase transport model. Zaveri et al.¹⁵ developed a comparable framework for describing gas–

particle SOA partitioning that accounts for diffusion and reaction in the particle phase and includes the size distribution dynamics of the aerosol population. Liu et al.¹⁶ presented an exact analytical solution of the transient equations of gas-phase diffusion of a condensing vapor to and diffusion and first-order reaction in a particle. These three studies provide the theoretical and computational framework to estimate the time scale for establishment of gas–particle equilibrium. The present work assesses the regimes of parameter values associated with various limiting cases of gas–particle transport. On the basis of the analytical solution of Liu et al.,¹⁶ we derive expressions for the time scales associated with the transport steps involved in SOA growth. We evaluate the overall time scale to achieve gas–particle equilibrium in both open and closed systems and compare it to that obtained from the full numerical solution of Shiraiwa and Seinfeld.¹⁴

2. ANALYTICAL SOLUTION FOR TRANSIENT GAS–PARTICLE PARTITIONING

Transport of a vapor molecule to a particle involves three mass transfer processes that occur in series: (1) diffusion from the bulk of the gas phase to the particle surface, (2) transport across the gas–particle interface, and (3) diffusion into the interior of the particle. If reactions are occurring in the particle

Received: May 27, 2015

Revised: August 25, 2015

Accepted: September 4, 2015

Published: September 4, 2015

phase, these occur simultaneously with particle-phase diffusion. In the present work, we do not explicitly consider the effect of chemical reactions. Any of these three processes can be rate-determining, depending on the particular set of conditions, and the rate-determining step will govern the time scale for achieving gas–particle equilibrium. The mathematical statement of the transport problem joins gas-phase diffusion, accommodation at the particle surface, and diffusion into the particle bulk. It is assumed that at $t = 0$ the particle is free of the condensing species and that the bulk gas-phase concentration of the condensing species is maintained as constant for $t > 0$. This latter condition restricts the analytical solution to a so-called open system, one in which the bulk vapor concentration is maintained at a constant level. In the corresponding closed system, the total amount of vapor available is fixed so that as condensation occurs the vapor concentration decreases. The exact analytical solution of the coupled gas and particle phase transport problem allows one to derive the expression for the overall time scales to achieve equilibrium, from which one can infer which transport step controls the overall approach to equilibrium. A general numerical simulation that treats both open and closed systems, such as that used by Shiraiwa and Seinfeld,¹⁴ can account for change of particle size with condensation and generation or depletion of the vapor by chemical reaction.

We consider the analytical formulation for transient gas–particle partitioning of a species with a fixed concentration in the bulk gas phase into a particle free of that species at $t = 0$. Letting $G(r, t)$ and $A(r, t)$ be the gas- and particle-phase concentrations of the transporting species, the transient boundary value problem describing the approach to equilibrium is¹⁶

$$\frac{\partial A(r, t)}{\partial t} = D_b \left[\frac{\partial^2 A(r, t)}{\partial r^2} + \frac{2}{r} \frac{\partial A(r, t)}{\partial r} \right] \quad (1)$$

$$\begin{aligned} D_g \left(\frac{\partial G}{\partial r} \right)_{r=R_p} &= \frac{1}{4} \alpha \bar{v} \left[G(R_p, t) - \frac{A(R_p, t)}{H'} \right] \\ &= D_b \left(\frac{\partial A}{\partial r} \right)_{r=R_p} \end{aligned} \quad (2)$$

$$G(r, t) = G_\infty - \frac{R_p}{r} [G_\infty - G(R_p, t)] \quad (3)$$

$$A(r, 0) = 0 \quad (4)$$

$$\left(\frac{\partial A(r, t)}{\partial r} \right)_{r=0} = 0 \quad (5)$$

where G_∞ is the bulk gas-phase concentration of the condensing species, R_p is the particle radius, α is the accommodation coefficient of the condensing species on the particle surface, \bar{v} is the mean molecular speed of the condensing species in the gas phase, D_g is the molecular diffusion coefficient of the condensing species in the gas phase, D_b is the molecular diffusivity of the condensing species in the particle phase, and H' is the dimensionless Henry's law constant for the condensing species ($H' = H_A RT$). Equation 3 expresses the steady-state diffusion profile in the gas phase. Under any circumstances, the time scale to establish a steady-state concentration profile in the gas phase is extremely short;

therefore, the steady-state gas-phase profile for the condensing species holds at all times.¹⁷

The use of a Henry's law constant is customary when describing the equilibrium of a dissolved solute in a relatively dilute cloud droplet. Here, our primary interest concerns the equilibrium of a solute between the gas phase and a submicrometer aerosol particle, for which a gas–particle equilibrium constant formulation is customary.¹ The two formulations for equilibrium can be related as follows. Assuming an ideal mixture, the equilibrium partial pressure of condensing species A is $p_A = x_A p_A^\circ$, where p_A° is the saturation vapor pressure of species A and x_A is the mole fraction of A in the particle phase. The mole fraction of the condensing species A is related to the mass fraction in the gas-phase, $x_A = (A^g/c^*)$, where A^g is the mass concentration of condensing species A in the gas phase ($\text{g (m}^3 \text{ of air)}^{-1}$) and c^* is the saturation mass concentration of the condensing species. Assuming that the molecular weight of the condensing species A is identical to that of the absorbing particle phase and that individual condensing species A is one of many in the particle phase, the mole fraction of A can be written as

$$x_A \approx \frac{A^p}{c_{OA} + A^p} \approx \frac{A^p}{c_{OA}}$$

where A^p is the mass concentration of condensing species A in the particle phase ($\text{g (m}^3 \text{ of air)}^{-1}$) and c_{OA} is the mass concentration of absorbing phase ($\text{g (m}^3 \text{ of air)}^{-1}$). Thus, the distribution factor f_A , the ratio of particle-phase mass concentration to the gas-phase mass concentration, is

$$f_A = \frac{A^p}{A^g} = \frac{c_{OA}}{c^*}$$

and $f_A = H_A RT w_L = H' w_L$, where H_A is Henry's law constant (M atm^{-1}) and w_L is volume fraction of particle in the air (m^3 of particle (m^3 of air) $^{-1}$). Thus, the partitioning equilibrium constant is

$$K_p = \frac{A^p/c_{OA}}{A^g} = \frac{1}{c^*}$$

and the dimensionless Henry's law constant H' is formally related to the gas–particle partitioning equilibrium by

$$H' = K_p \frac{c_{OA}}{w_L} = K_p \rho_p$$

where ρ_p is the density of particle ($\text{g (m}^3 \text{ of particle)}^{-1}$). The equilibrium fraction of organic material in the particle phase is $(1 + c^*/c_{OA})^{-1}$. Thus, for $c_{OA} = 1 \mu\text{g m}^{-3}$, a condensing substance with $c^* = 1 \mu\text{g m}^{-3}$ will reside 50% in the particle phase at equilibrium; a substance with $c^* = 0.01 \mu\text{g m}^{-3}$ will reside 99% in the particle phase.

The solution for the normalized particle-phase concentration of the condensing species defined by eqs 1–5 is¹⁵

$$\phi(\eta, \theta) = 1 - \frac{2}{\eta} \sum_{n=1}^{\infty} \frac{L e^{-\beta_n^2 \theta} \sin(\beta_n \eta)}{[\beta_n^2 + L(L-1)] \sin \beta_n} \quad (6)$$

where $\phi = (A(r, t)/A_\infty)$, $\eta = (r/R_p)$, $\theta = (D_b t)/R_p^2$, and $A_\infty = H' G_\infty$ and A_∞ is the particle-phase concentration of the condensing species at equilibrium with the gas-phase concentration G_∞ . β_n is the n th positive root of

$$\beta \cot \beta + L - 1 = 0 \quad (7)$$

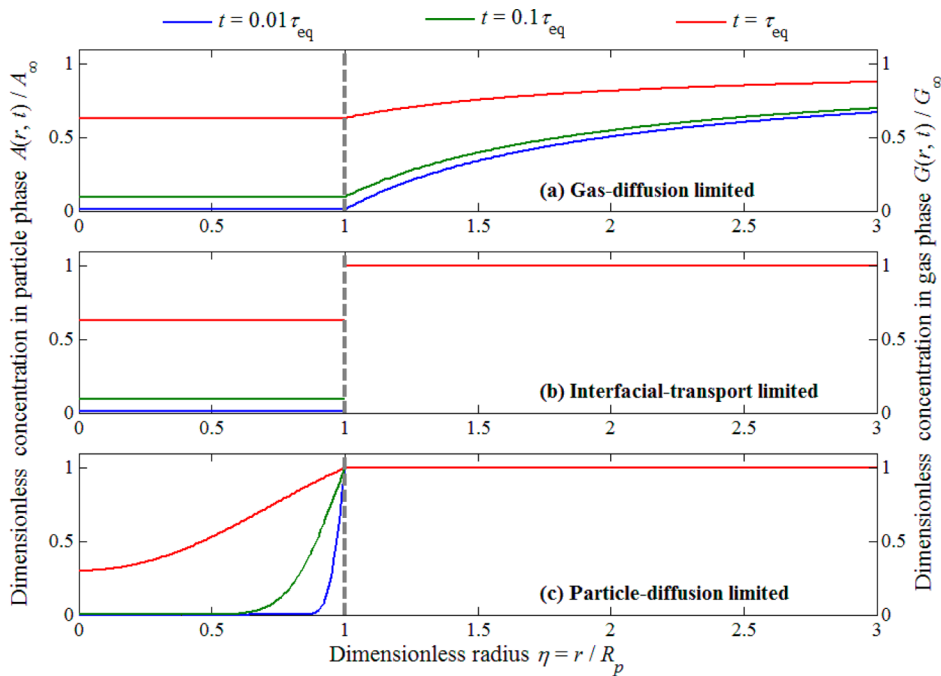


Figure 1. Dimensionless concentration profiles in the particle and gas phase for three limiting cases: (a) gas-phase diffusion-limited partitioning, (b) interfacial-transport-limited partitioning, and (c) particle-phase diffusion-limited partitioning. The region $\eta \leq 1$ corresponds to the particle phase.

where

$$L = \frac{\nu_b^{-1}}{\nu_i^{-1} + \nu_g^{-1}} \tag{8}$$

and the transport velocities for gas-phase diffusion, interfacial transport, and particle-phase diffusion, respectively, are

$$\nu_g = \frac{D_g}{R_p H'}, \quad \nu_i = \frac{\alpha \bar{v}}{4H'}, \quad \text{and} \quad \nu_b = \frac{D_b}{R_p} \tag{9}$$

Physically, a limit of $L \gg 1$ implies that transport in the particle phase is much slower than that in the gas phase or across the interface, and a limit of $L \ll 1$ corresponds to the case in which particle-phase diffusion is rapid relative to either gas-phase diffusion or interfacial accommodation.

The time-dependent gas-phase concentration profile of the condensing species is obtained from eq 6 on the basis of the equality of fluxes, eq 2

$$\frac{G(\eta, \theta)}{G_\infty} = 1 - \frac{1}{\eta} \left[2 \sum_{n=1}^{\infty} \frac{L e^{-\beta_n^2 \theta}}{\beta_n^2 + L(L-1)} - \frac{8H'D_b}{\alpha \bar{v} R_p} \sum_{n=1}^{\infty} \frac{L^2 e^{-\beta_n^2 \theta}}{\beta_n^2 + L(L-1)} \right] \tag{10}$$

The e -folding time scale to achieve overall gas-particle equilibrium partitioning is approximated by the exponent in the first term of the infinite series in eq 6.

$$\tau_{eq} = \frac{R_p^2}{\beta_1^2 D_b} \tag{11}$$

This time scale represents that for the entire particle to achieve equilibrium with the bulk gas-phase concentration G_∞ . Three important limits can be identified on the basis of eq 11.

If the transport resistance is dominated by gas-phase diffusion, i.e., $\nu_g \ll \nu_i$ and $\nu_g \ll \nu_b$, then

$$L \cong \frac{D_g}{H'D_b} \ll 1 \tag{12}$$

and $\beta_1 \cong (3L)^{1/2} \ll 1$. In this case, both interfacial equilibrium and a uniform particle-phase concentration are established (Figure 1a). Letting $L \rightarrow 0$ in eq 6, $\lim_{L \rightarrow 0^+} \phi(\eta, \theta) = 1 - e^{-3L\theta}$, the time-dependent dimensionless concentration of the condensing species in the particle phase is

$$\phi(\eta, \theta) = 1 - \exp\left(-\frac{3D_g}{H'R_p^2} t\right) \tag{13}$$

and the equilibrium partitioning time scale is governed by diffusion in the particle phase,

$$\tau_{eq} = H' \frac{R_p^2}{3D_g} \tag{14}$$

If the transport resistance is dominated by interfacial accommodation, i.e., $\nu_i \ll \nu_g$ and $\nu_i \ll \nu_b$, then the parameter L can be approximated as

$$L \cong \frac{\alpha \bar{v} R_p}{4H'D_b} \ll 1 \tag{15}$$

In this limiting case, the concentration profiles of the condensing species in both the gas and particle phases are essentially uniform, owing to relatively rapid particle-phase diffusion (Figure 1b). The form of the dimensionless concentration of the condensing species in the particle phase in this limit is

Table 1. Examples of Three Limiting Cases^a

	gas-phase-diffusion-limited partitioning	interfacial-transport-limited partitioning	particle-phase-diffusion-limited partitioning
R_p (μm)	10	0.05	0.05
D_b ($\text{cm}^2 \text{s}^{-1}$)	10^{-5}	10^{-9}	10^{-18}
α	1	10^{-3}	10^{-2}
	$\nu_g/\nu_i = 2.25 \times 10^{-2}$	$\nu_i/\nu_g = 2.2 \times 10^{-4}$	$\nu_b/\nu_g = 10^{-6}$
	$\nu_g/\nu_b = 10^{-7}$	$\nu_i/\nu_b = 2.2 \times 10^{-7}$	$\nu_b/\nu_i = 4.5 \times 10^{-4}$

^a $c^* = 10 \mu\text{g m}^{-3}$; $M = 200 \text{ g mol}^{-1}$; $D_g = 0.1 \text{ cm}^2 \text{ s}^{-1}$; and $H' = 10^{11}$. Because H' and c^* are related by $H' = \rho_p/c^*$, where ρ_p is the density of the particle, $c^* = 10 \mu\text{g m}^{-3}$ corresponds to $H' = 10^{11}$, given $\rho_p = 1 \text{ g cm}^{-3}$.

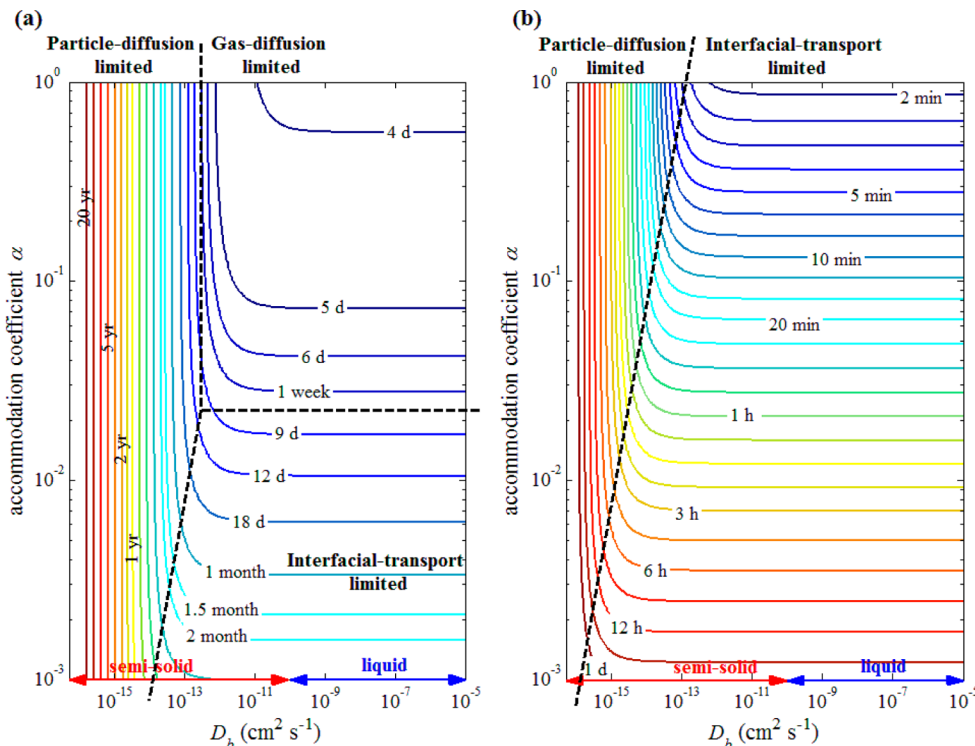


Figure 2. Analytical equilibrium partitioning time scale as a function of particle-phase diffusivity D_b and accommodation coefficient α for two particle diameters: (a) $20 \mu\text{m}$ and (b) 100 nm . Other physical parameters are identical for the two panels: $M = 200 \text{ g mol}^{-1}$, $D_g = 10^{-1} \text{ cm}^2 \text{ s}^{-1}$, $H' = 10^{11}$.

$$\lim_{L \rightarrow 0^+} \phi(\eta, \theta) = 1 - \exp\left(-\frac{3\alpha\bar{v}}{4H'R_p}t\right) \tag{16}$$

$$\tau_{\text{eq}} = \frac{R_p^2}{\pi^2 D_b} \tag{20}$$

and the equilibrium partitioning time scale in this case is

$$\tau_{\text{eq}} = H' \frac{4R_p}{3\alpha\bar{v}} \tag{17}$$

If the overall transport resistance is dominated by particle-phase diffusion, i.e., $\nu_b \ll \nu_g$ and $\nu_b \ll \nu_i$, then eq 7 reduces to

$$\beta_n = n\pi \left(1 - \frac{1}{L-1}\right) \tag{18}$$

and

$$\lim_{L \rightarrow 0^+} \phi(\eta, \theta) = 1 - \frac{2}{\eta} \sum_{n=1}^{\infty} \frac{(-1)^{n-1}}{n\pi} e^{-n^2\pi^2\theta} \sin(n\pi\eta) \tag{19}$$

The equilibrium partitioning time scale in this limit, depicted in Figure 1c, is simply that associated with diffusion in the particle phase

Table 1 presents parameter values that illustrate the three limiting regimes of gas–particle equilibration. In each case, we consider an organic species with saturation mass concentration $c^* = 10 \mu\text{g m}^{-3}$, molecular weight $M = 200 \text{ g mol}^{-1}$, and a gas-phase molecular diffusivity $D_g = 10^{-1} \text{ cm}^2 \text{ s}^{-1}$. Gas-phase-diffusion-limited partitioning is likely to occur for large liquid particles (i.e., droplets) with a vapor accommodation coefficient α close to 1.0. Interfacial-transport-limited partitioning will hold for small, somewhat viscous particles with a relatively small vapor accommodation coefficient. Finally, particle-phase-diffusion-limited partitioning is expected to occur for highly viscous (e.g., semisolid) aerosols.

3. RESULTS AND DISCUSSION

3.1. Analytical Time Scales. Figure 2 shows the dependence of the analytical gas–particle partitioning time scale τ_{eq} on particle-phase diffusivity D_b and accommodation coefficient α for cloud droplets (Panel (a): $D_p = 20 \mu\text{m}$) and fine-mode aerosols (Figure 2b, $D_p = 100 \text{ nm}$). The dashed lines in Figure 2 are intended to give a rough indication of the

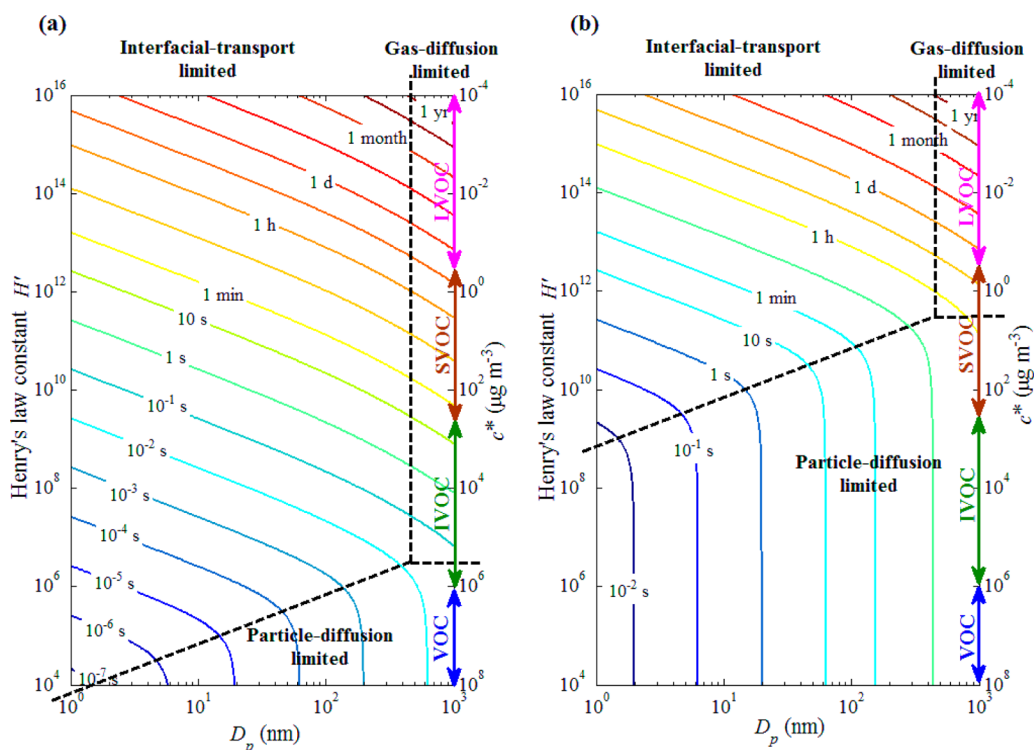


Figure 3. Analytical equilibrium partitioning time scale as a function of particle diameter D_p and Henry's law constant H' (or equivalent saturation mass concentration c^*). (a) Liquid particles; $D_b = 10^{-8} \text{ cm}^2 \text{ s}^{-1}$. (b) Highly viscous particles; $D_b = 10^{-13} \text{ cm}^2 \text{ s}^{-1}$. Other physical parameters are identical for the two panels: $M = 200 \text{ g mol}^{-1}$, $D_g = 10^{-1} \text{ cm}^2 \text{ s}^{-1}$, $\rho_p = 1 \text{ g cm}^{-3}$, $\alpha = 1$.

location of the transition regions between those representing different controlling mechanisms. Although our principal interest in this work is the equilibration behavior of organic atmospheric aerosols, it is also informative to examine the implications of the theory for typical cloud droplets. The equilibration time scale for a solute dissolving in a cloud droplet with typical aqueous-phase diffusivities is gas-phase diffusion controlled for values of $\alpha = 0.01$. Because of the relatively large size of cloud droplets, theoretical gas–droplet equilibration time scales are much longer than the typical lifetime of a cloud droplet. Most relevant for the present work is Figure 2b. For particles in the size range of typical atmospheric organic aerosols ($\sim 50\text{--}500 \text{ nm}$), the gas–particle equilibration time scale is governed by either interfacial accommodation or particle-phase diffusion. For $\alpha \gtrsim 0.01$ and $D_b \lesssim 10^{-13} \text{ cm}^2 \text{ s}^{-1}$, gas–particle equilibration is controlled by particle-phase diffusion. When $\alpha \lesssim 0.01$, interfacial accommodation is controlling, and τ_{eq} is asymptotically proportional to α . For $\alpha \gtrsim 0.1$, the time scale for a fine mode aerosol particle to achieve gas–particle equilibrium is on the order of minutes for all but the smallest particle-phase diffusion coefficients. For submicrometer atmospheric aerosols, gas-phase diffusion of the condensing species is not a limiting process to achieve gas–particle equilibrium. The transitional boundaries between limiting regimes can be defined approximately by the intersection of the corresponding asymptotic solutions. For example, a rough indication of the particle size range where the transition between gas-phase-diffusion-limited and interfacial-transport-limited regimes occurs can be obtained by combining eqs 14 and 17.

$$R_p = \frac{4D_g}{\alpha\bar{v}} \quad (21)$$

Figure 3 shows τ_{eq} as a function of particle diameter D_p and Henry's law constant H' and c^* with $\alpha = 1.0$. Figure 3a is for $D_b = 10^{-8} \text{ cm}^2 \text{ s}^{-1}$, and Figure 3b is for $D_b = 10^{-13} \text{ cm}^2 \text{ s}^{-1}$. For SOA, the gas–particle equilibrium state is commonly characterized by the gas-phase saturation mass concentration c^* and the gas–particle partitioning equilibrium constant K_p , which as we have shown can be related to H' . τ_{eq} increases with particle diameter because the smaller surface area per unit volume for larger particles is less efficient for vapor uptake. Gas–particle partitioning between a highly volatile organic compound ($c^* \gtrsim 10^6 \mu\text{g m}^{-3}$) and a liquid particle (Figure 3a) is rapid. If the condensing species is less volatile, then more material ultimately condenses into the particle at equilibrium. The larger amount of condensing material must be transported into the particle through the gas phase and the interface, which leads to a longer equilibration time. Because particle-phase diffusion alone does not depend on the volatility of the condensing species, the limiting step changes from particle-phase diffusion toward interfacial transport or gas-phase diffusion for low volatility species. Figure 3b presents the comparable calculation for a highly viscous particle. Owing to hindered diffusion in the particle phase, equilibration times are longer than in the liquid particle for the same particle size and species volatility.

3.2. Numerical Simulation in Open and Closed Systems. An alternative to the analytical evaluation of equilibration time scales is detailed numerical simulation of the process of vapor molecule diffusion to and uptake in a particle or a population of particles. The kinetic multilayer model (KM-GAP)^{18,19} for gas–particle interactions in aerosols and clouds allows evaluation of τ_{eq} by numerically simulating the evolution of the condensing species concentrations in gas and particle phases.¹⁴ The model is general in terms of whether

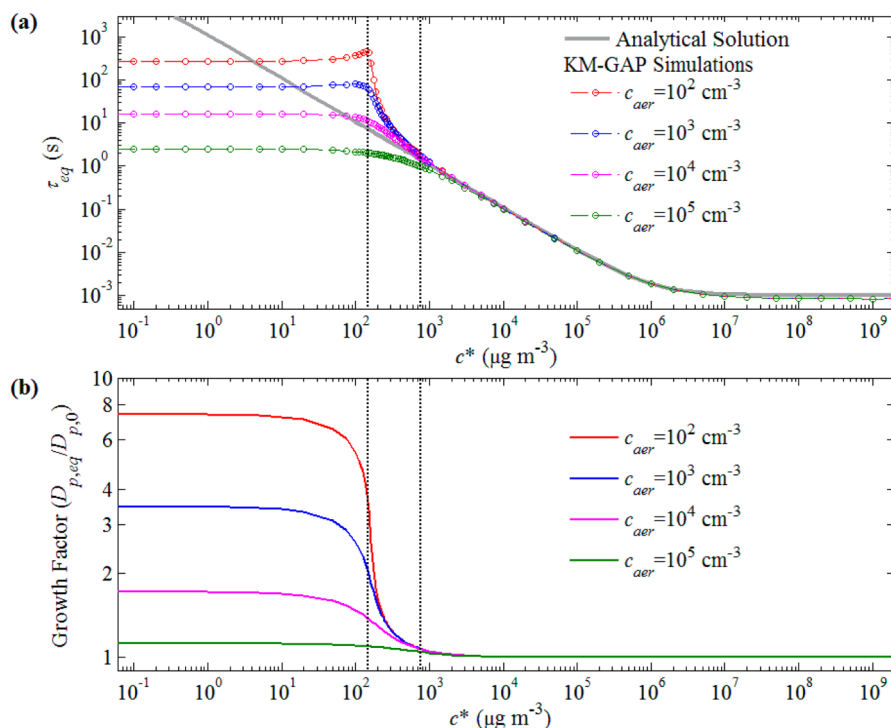


Figure 4. Effect of an open vs closed system. The analytical equilibration time scale for the open system is given by eq 11. The equilibration time scale for the closed system is computed by the KM-GAP numerical model. (a) Equilibrium partitioning time scale as a function of saturation mass concentration c^* at different particle number concentrations c_{aer} for both open and closed systems. (b) Equilibrium particle growth factor in the closed system as a function of particle number concentration from KM-GAP. Physical parameters used in the KM-GAP model simulations are $\alpha = 1.0$, $\tau_d = 10^{-9}$ s, $\rho_p = 1$ g cm^{-3} , $D_b = 10^{-8}$ cm^2 s^{-1} , $D_g = 10^{-1}$ cm^2 s^{-1} , $M = 200$ g mol^{-1} , and $D_{p,0} = 200$ nm.

the overall system is open (vapor concentration maintained as constant) or closed (finite amount of vapor). The analytical solution above assumes an open system, i.e., the bulk gas-phase concentration of the condensing species is constant. In a closed system, the bulk gas-phase concentration decreases as condensation into the aerosol phase proceeds.

It is instructive to compare the analytical approximation for τ_{eq} on the basis of eq 11 with that derived from numerical simulation using KM-GAP. We consider numerical simulation of a population of particles growing in open and closed systems. For simplicity, gas- and particle-phase chemical reactions are not considered in this comparison. Figure 4a shows the equilibrium partitioning time scale as a function of saturation mass concentration c^* at different particle number concentrations c_{aer} in a closed system. The analytical approximation and the numerical simulation are essentially identical for relatively volatile species, $c^* \gtrsim 10^3$ $\mu\text{g m}^{-3}$. The analytical prediction based on the assumption of a fixed bulk gas-phase concentration of the condensing species and the numerical simulation based on a closed system in which the bulk concentration declines with time begin to diverge for $c^* \lesssim 10^3$ $\mu\text{g m}^{-3}$. This divergence is the result of two effects that are not explicitly treated in the analytical solution: (1) particle size change (The KM-GAP model tracks the change of particle size due to condensation of vapor.) and (2) vapor depletion (In a closed system, as vapor condenses on the particle, the bulk gas-phase concentration decreases.) Each of these two effects becomes negligible for a sufficiently volatile condensing species ($c^* \gtrsim 10^3$ $\mu\text{g m}^{-3}$) because an overall smaller amount of vapor species condenses into the particles. Consequently, the gas-particle equilibrium time scale computed from KM-GAP shows no dependence on the aerosol number concentration c_{aer} in this

region. For condensing species with a saturation mass concentration in the range 2×10^2 $\mu\text{g m}^{-3} \lesssim c^* \lesssim 10^3$ $\mu\text{g m}^{-3}$, the discrepancy between the open and closed system arises from the effect of particle growth. The equilibrium particle size increases dramatically in this region, as shown in Figure 4b, so the actual time for the system to achieve gas-particle equilibrium can be considerably longer than that estimated on the basis of the initial particle size. For decreasing particle concentration c_{aer} , the equilibrium particle size increases, because a greater amount of vapor condenses into each particle. For number concentrations characteristic of urban conditions ($c_{aer} = 10^5$ cm^{-3}), the condensing vapor is distributed over a relatively large number of particles, and the effect of particle size change on the equilibration time scale is negligible, as shown in Figure 4b. However, in the closed system, the effect of gas-phase depletion begins to dominate the equilibrium time scale: As the vapor becomes depleted, a progressively smaller amount of vapor transfers into the particle phase, and the equilibrium time scale decreases.

For less volatile vapor, $c^* \lesssim 2 \times 10^2$ $\mu\text{g m}^{-3}$, in the closed system, gas-particle partitioning is dominated by gas-phase depletion of the condensing species. Less volatile condensing species transfer predominantly into the particle phase, and as volatility decreases, τ_{eq} and the equilibrium particle size eventually become independent of the volatility of the condensing species because virtually all of it effectively condenses.

3.3. Implications for Atmospheric Models. Atmospheric models simulate the formation and growth of organic aerosols. At present, these processes are assumed in most models to be the result of instantaneous gas-particle equilibrium. In addition, most atmospheric models do not resolve the ambient

aerosol size distribution. Under a number of ambient situations, the rate at which that equilibrium is achieved can be slower than the rates at which other atmospheric processes are changing. The numerical machinery needed to resolve these microscopic gas–particle interactions would add substantially to an already heavy computational load. Using a combination of analytical transport theory and numerical modeling, the present work delineates the broad conditions governing the time scales for establishing gas–particle equilibrium. These conditions depend on the surface accommodation coefficient and volatility of the species in question, the diffusivity of the condensing organic species in the particle phase, and the particle size. In most ambient modeling circumstances, surface accommodation coefficients for condensing species and viscosities of particles (from which diffusion coefficients have to be inferred) are not known with precision. Thus, a high degree of uncertainty will attend any computation based on microscopic particle dynamics; nonetheless, the results of the present work provide a framework for estimation of the possible effect of non-equilibrium growth in atmospheric models of organic aerosols.

AUTHOR INFORMATION

Corresponding Author

*E-mail: seinfeld@caltech.edu. Phone: (626) 395-4635.

Notes

The authors declare no competing financial interest.

ACKNOWLEDGMENTS

This work was supported by National Science Foundation grant AGS-1523500.

REFERENCES

- (1) Seinfeld, J. H.; Pankow, J. F. Organic atmospheric particulate material. *Annu. Rev. Phys. Chem.* **2003**, *54*, 121–140.
- (2) Grieshop, A. P.; Donahue, N. M.; Robinson, A. L. Is the gas–particle partitioning in alpha-pinene secondary organic aerosol reversible? *Geophys. Res. Lett.* **2007**, *34*, L14810.
- (3) Vaden, T. D.; Song, C.; Zaveri, R. A.; Imre, D.; Zelenyuk, A. Morphology of mixed primary and secondary organic particles and the adsorption of spectator organic gases during aerosol formation. *Proc. Natl. Acad. Sci. U. S. A.* **2010**, *107*, 6658–6663.
- (4) Virtanen, A.; Joutsensaari, J.; Koop, T.; Kannosto, J.; Yli-Pirila, P.; Leskinen, J.; Makela, J. M.; Holopainen, J. K.; Poschl, U.; Kulmala, M.; Worsnop, D. R.; Laaksonen, A. An amorphous solid state of biogenic secondary organic aerosol particles. *Nature* **2010**, *467*, 824–827.
- (5) Pierce, J. R.; Riipinen, I.; Kulmala, M.; Ehn, M.; Petäjä, T.; Junninen, H.; Worsnop, D. R.; Donahue, N. M. Quantification of the volatility of secondary organic compounds in ultrafine particles during nucleation events. *Atmos. Chem. Phys.* **2011**, *11*, 9019–9036.
- (6) Vaden, T. D.; Imre, D.; Beránek, J.; Shrivastava, M.; Zelenyuk, A. Evaporation kinetics and phase of laboratory and ambient secondary organic aerosol. *Proc. Natl. Acad. Sci. U. S. A.* **2011**, *108*, 2190–2195.
- (7) Kuwata, M.; Martin, S. T. Phase of atmospheric secondary organic material affects its reactivity. *Proc. Natl. Acad. Sci. U. S. A.* **2012**, *109*, 17354–17359.
- (8) Perraud, V.; Bruns, E. A.; Ezell, M. J.; Johnson, S. N.; Yu, Y.; Alexander, M. L.; Zelenyuk, A.; Imre, D.; Chang, W. L.; Dabdub, D.; Pankow, J. F.; Finlayson-Pitts, B. J. Nonequilibrium atmospheric secondary organic aerosol formation and growth. *Proc. Natl. Acad. Sci. U. S. A.* **2012**, *109*, 2836–2841.
- (9) Abramson, E.; Imre, D.; Beránek, J.; Wilson, J.; Zelenyuk, A. Experimental determination of chemical diffusion within secondary organic aerosol particles. *Phys. Chem. Chem. Phys.* **2013**, *15*, 2983–2991.
- (10) Saukko, E.; Lambe, A. T.; Massoli, P.; Koop, T.; Wright, J. P.; Croasdale, D. R.; Pedernera, D. A.; Onasch, T. B.; Laaksonen, A.; Davidovits, P.; Worsnop, D. R.; Virtanen, A. Humidity-dependent phase state of SOA particles from biogenic and anthropogenic precursors. *Atmos. Chem. Phys.* **2012**, *12*, 7517–7529.
- (11) Renbaum-Wolff, L.; Grayson, J. W.; Bertram, A. K. Technical Note: New methodology for measuring viscosities in small volumes characteristic of environmental chamber particle samples. *Atmos. Chem. Phys.* **2013**, *13*, 791–802.
- (12) Renbaum-Wolff, L.; Grayson, J. W.; Bateman, A. P.; Kuwata, M.; Sellier, M.; Murray, B. J.; Shilling, J. E.; Martin, S. T.; Bertram, A. K. Viscosity of α -pinene secondary organic material and implications for particle growth and reactivity. *Proc. Natl. Acad. Sci. U. S. A.* **2013**, *110*, 8014–8019.
- (13) Loza, C. L.; Coggon, M. M.; Nguyen, T. B.; Zuend, A.; Flagan, R. C.; Seinfeld, J. H. On the mixing and evaporation of secondary organic aerosol components. *Environ. Sci. Technol.* **2013**, *47*, 6173–6180.
- (14) Shiraiwa, M.; Seinfeld, J. H. Equilibration timescale of atmospheric secondary organic aerosol partitioning. *Geophys. Res. Lett.* **2012**, *39*, L24801.
- (15) Zaveri, R. A.; Easter, R. C.; Shilling, J. E.; Seinfeld, J. H. Modeling kinetic partitioning of secondary organic aerosol and size distribution dynamics: representing effects of volatility, phase state, and particle-phase reaction. *Atmos. Chem. Phys.* **2014**, *14*, 5153–5181.
- (16) Liu, A. T.; Zaveri, R. A.; Seinfeld, J. H. Analytical solution for transient partitioning and reaction of a condensing vapor species in a droplet. *Atmos. Environ.* **2014**, *89*, 651–654.
- (17) Seinfeld, J. H.; Pandis, S. N. *Atmospheric Chemistry and Physics: From Air Pollution to Climate Change*; John Wiley & Sons: Hoboken, NJ, 2006.
- (18) Pöschl, U.; Rudich, Y.; Ammann, M. Kinetic model framework for aerosol and cloud surface chemistry and gas–particle interactions – Part 1: General equations, parameters, and terminology. *Atmos. Chem. Phys.* **2007**, *7*, 5989–6023.
- (19) Shiraiwa, M.; Pfrang, C.; Koop, T.; Pöschl, U. Kinetic multi-layer model of gas–particle interactions in aerosols and clouds (KM-GAP): linking condensation, evaporation and chemical reactions of organics, oxidants and water. *Atmos. Chem. Phys.* **2012**, *12*, 2777–2794.